AFRL-AFOSR-JP-TR-2020-0025

Impact of Thermal Effects and Mechanical stress on the RF Performance of Flexible Transmit and Receive Modules

Koenraad Mouthaan
NATIONAL UNIVERSITY OF SINGAPORE
21 LOWER KENT RIDGE ROAD
SINGAPORE, 119077
SG

10/24/2020
Final Report

Air Force Research Laboratory
Air Force Office of Scientific Research
Asian Office of Aerospace Research and Development
Unit 45002, APO AP 96338-5002

REPORT DOCUMENTATION PAGE

Form Approved
OMB No. 0704-0188

1. REPORT DATE *(DD-MM-YYYY)*	2. REPORT TYPE	3. DATES COVERED *(From - To)*
24-10-2020	Final	15 Jun 2018 to 14 Jun 2020

4. TITLE AND SUBTITLE
Impact of Thermal Effects and Mechanical stress on the RF Performance of Flexible Transmit and Receive Modules

5a. CONTRACT NUMBER

5b. GRANT NUMBER
FA2386-18-1-4007

5c. PROGRAM ELEMENT NUMBER
61102F

6. AUTHOR(S)
Koenraad Mouthaan

5d. PROJECT NUMBER

5e. TASK NUMBER

5f. WORK UNIT NUMBER

7. PERFORMING ORGANIZATION NAME(S) AND ADDRESS(ES)
NATIONAL UNIVERSITY OF SINGAPORE
21 LOWER KENT RIDGE ROAD
SINGAPORE, 119077 SG

8. PERFORMING ORGANIZATION REPORT NUMBER

9. SPONSORING/MONITORING AGENCY NAME(S) AND ADDRESS(ES)
AOARD
UNIT 45002
APO AP 96338-5002

10. SPONSOR/MONITOR'S ACRONYM(S)
AFRL/AFOSR IOA

11. SPONSOR/MONITOR'S REPORT NUMBER(S)
AFRL-AFOSR-JP-TR-2020-0025

12. DISTRIBUTION/AVAILABILITY STATEMENT
A DISTRIBUTION UNLIMITED: PB Public Release

13. SUPPLEMENTARY NOTES

14. ABSTRACT
In the project Impact of Thermal Effects and Mechanical Stress on the Microwave Performance of Transmit and Receive Circuits on Flexible Substrates, funded by the Hybrid Integrated Flexible Electronic Systems (HiFES) program at the National University of Singapore, and by AOARD, basic research was undertaken to investigate feasibility of active radio frequency (RF) circuits on flexible substrates, for application in flexible phased array antennas.

15. SUBJECT TERMS
thermal effects, radio frequency (RF), mechnical stress, flexible substrates

16. SECURITY CLASSIFICATION OF:			17. LIMITATION OF ABSTRACT	18. NUMBER OF PAGES	19a. NAME OF RESPONSIBLE PERSON
a. REPORT	b. ABSTRACT	c. THIS PAGE			KNOPP, JEREMY
Unclassified	Unclassified	Unclassified	SAR		19b. TELEPHONE NUMBER *(Include area code)* 315-227-7006

Standard Form 298 (Rev. 8/98)
Prescribed by ANSI Std. Z39.18

Title	Impact of Thermal Effects and Mechanical stress on the RF Performance of Flexible Transmit and Receive Modules
AOARD Grant	FA2386-18-1-4007
Type	Final Report
Date	October 22, 2020
Name of PI	Koenraad Mouthaan
E-mail address	k.mouthaan@nus.edu.sg
Institution	National University of Singapore
Mailing Address	4 Engineering Drive 3 Singapore 117583
Phone	(+65)-6516-4936
Fax	(+65)-6779-1103
Period of Performance Month/Day/Year-Month/Day/Year	06/15/2018 – 06/14/2020

This material is based on research sponsored by the Air Force Research Laboratory, under agreement number FA2386-18-1-4007. The U.S. Government is authorized to reproduce and distribute reprints for governmental purposes notwithstanding any copyright notation thereon. The views and conclusions contained herein are those of the authors and should not be interpreted as necessarily representing the official policies or endorsements, either expressed or implied, of the Air Force Research Laboratory or the U.S. Government.

Table of Contents

Chapter 1. Summary

With the increasing demand for radar sensing and wireless communication, in particular in the aerospace and automotive industry, conformal antennas have attracted significant attention. Recent technological advances in flexible electronics may enable the development of simple to fabricate, low-cost, lightweight, antenna systems, which are conformable to a wide variety of form factors. This is especially important since curved shapes are used for reasons of aerodynamics, low-detectability, and aesthetics. Conformal antenna technology may enable highly integrated, compact and low-profile active antenna arrays. It is noted that planar and rigid substrates can be used to realize conformal antennas by using a faceting approach. However, such antennas can't be fully conformed to surfaces, necessitating research into flexible antennas.

In the project "Impact of Thermal Effects and Mechanical Stress on the Microwave Performance of Transmit and Receive Circuits on Flexible Substrates", funded by the Hybrid Integrated Flexible Electronic Systems (HiFES) program at the National University of Singapore, and by AOARD, basic research was undertaken to investigate feasibility of active radio frequency (RF) circuits on flexible substrates, for application in flexible phased array antennas.

In Chapter 3, passive conformal patch antennas at 2.4 GHz are presented. In chapter 3 a 2x2 array integrated with a commercially available low noise amplifier (LNA) is demonstrated. And in chapter 5 the initial design of a phased array system is discussed. At that stage, the active components are not yet integrated on the flexible substrate. Finally, chapter 6 concludes the report and provides recommendations for future research.

Chapter 2. Introduction

With the increasing demand for radar sensing and wireless communication, in particular in the aerospace and automotive industry, conformal antennas have attracted significant attention. Recent technological advances in flexible electronics may enable the development of simple to fabricate, low-cost, lightweight, antenna systems, which are conformable to a wide variety of form factors. This is especially important since curved shapes are used for reasons of aerodynamics, low-detectability, and aesthetics. Conformal antenna technology may enable highly integrated, compact and low-profile active antenna arrays. It is noted that planar and rigid substrates can be used to realize conformal antennas by using a faceting approach. However, such antennas can't be fully conformed to surfaces, necessitating research into flexible antennas.

At the National University of Singapore, the Hybrid Integrated Flexible Electronic Systems (HiFES) program was started in 2018. Within this program, seed funding was made available to enable researchers to investigate novel technologies and applications for flexible electronics in various areas, such as healthcare and antenna engineering.

In the project "Impact of Thermal Effects and Mechanical Stress on the Microwave Performance of Transmit and Receive Circuits on Flexible Substrates", funded by HiFES and AOARD, basic research was undertaken to investigate feasibility of active radio frequency (RF) circuits on flexible substrates, for application in flexible phased array antennas.

Although there are various candidates for the required flexible microwave substrate, results for sponge silicone rubber are reported here. Also, given the unknown microwave performance of the selected substrate, designs were made for the 2.4 GHz ISM band. Initial investigations showed that the selected microwave substrate is more lossy than

standard microwave substrates, but that these losses are still in the manageable range. Also, many components are commercially available at 2.4 GHz.

In Chapter 3, passive conformal patch antennas at 2.4 GHz are presented. The results from that chapter form the basis for the development of antennas integrated with microwave components. In chapter 4 a 2x2 array integrated with a commercially available low noise amplifier (LNA) is demonstrated. And in chapter 5 the initial design of a phased array system is discussed. At that stage, the active components are not yet integrated on the flexible substrate. Finally, chapter 6 concludes the report and provides recommendations for future research.

Chapter 3. Conformal and Lightweight 2.4 GHz ISM Band Patch Antenna on Silicone Sponge Rubber

3.1. Introduction

The demand for low-cost and lightweight flexible electronics is increasing, driven by new applications in wearables, automotive, and aerospace. Many of such applications require wireless communication or sensing at microwave frequencies. Consequently, the demand for conformable antennas is also increasing. Several approaches for conformable antennas have been investigated [1]-[7]. As weight, cost, conformability, robustness, and flexibility are essential requirements, polymer substrates provide a promising solution. Several polymers have been investigated, such as polydimethylsiloxane (PDMS) [4], [5], liquid crystal polymer (LCP) [6], polyimide foil [3], [7], polyethylene terephthalate (PET) [8], thermoplastic polyurethane (TPU) [9], as well as silicone rubber [10], [11]. The second requirement is that losses in the antenna are kept low to ensure relatively high antenna efficiencies. Therefore, substrate losses must be considered when selecting the polymer material. Materials such as bulk TPU or PDMS exhibit relatively large loss tangents, while polyimide and PET lose their flexibility when the thickness is increased.

An interesting candidate is silicone-based substrate, as it is a low-cost substrate available commercial off-the-shelf (COTS). In bulk form, its loss tangent is comparable to that of PDMS. To reduce substrate losses, a low-density flexible silicone sponge rubber (SSR) is considered here. This substrate is made of a silicone matrix infused with tiny air bubbles, resulting in a lightweight, porous, flexible substrate. SSR has several advantages compared to bulk silicone. The loss tangent tan δ of SSR is 0.006 at 2.45 GHz, compared to 0.0115 for bulk silicone. The lower tan δ will reduce substrate losses and increase antenna performance. The dielectric constant ε_r of SSR is 1.54 at 2.45 GHz, compared to 2.9 for bulk

silicone. And the material density of SSR is 0.25 g·cm^{-3}, compared to typically 1.2 g·cm^{-3} for bulk silicone.

This reduction in density by 80% enables a lightweight antenna. Lastly, the hardness of SSR is 11 Shore A, compared to typically 60 Shore A for silicone. Exploiting the favorable characteristics of SSR, a lightweight and easy to conform ISM band patch antenna is presented. Three options for the ground plane are investigated. Measurements are reported of the antenna with these options on a flat surface and conformed to three different cylindrical surfaces. Section 3.2 presents the design and simulation of the antenna as well as details the fabrication process. Section 3.3 focuses on the performance of the antenna, both in flat and conformal configurations for all ground plane options. The results are discussed in the section 3.4, and conclusions are provided in Section 3.5.

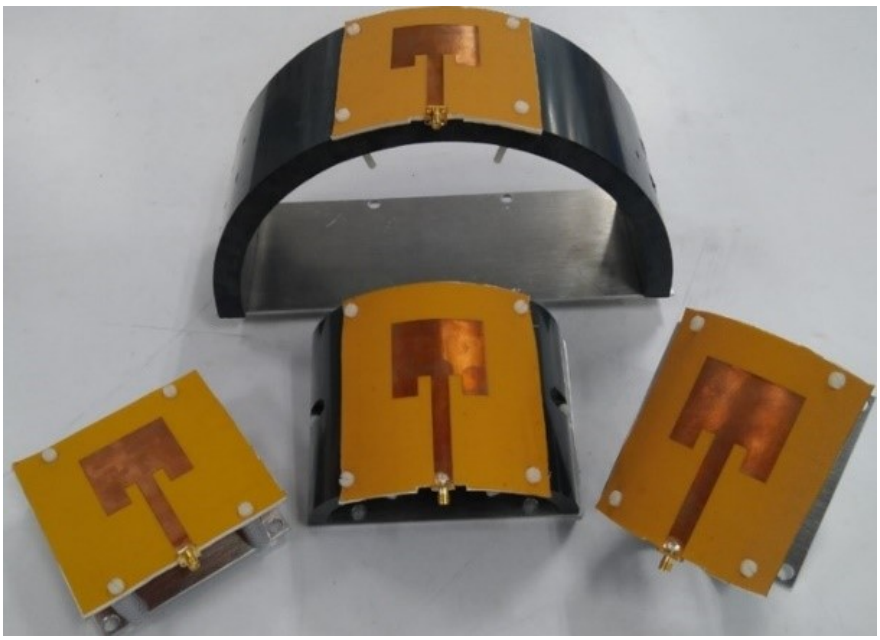

Fig. 3.1. Fabricated conformal antennas on a flat surface and cylindrical surfaces with radius R = 160 mm, R = 80 mm, and R = 40 mm.

3.2. Antenna design, simulation, and fabrication

The microstrip patch antenna is designed for the 2.4 GHz ISM band. This band is extensively used for license-free communication applications such

as Bluetooth, WiFi, and Zigbee. Three layers are used for the antenna, as follows. For the top layer, a flexible 60 μm polyimide PCB with copper cladding is used. The patch antenna is realized through standard PCB manufacturing techology. For the substrate, a flexible (11 Shore A) porous SSR sheet of 3 mm thickness is used. The SSR is backed by pressure sensitive adhesive (PSA). The top PCB is laminated on the SSR sheet using 3M 467MP adhesive.

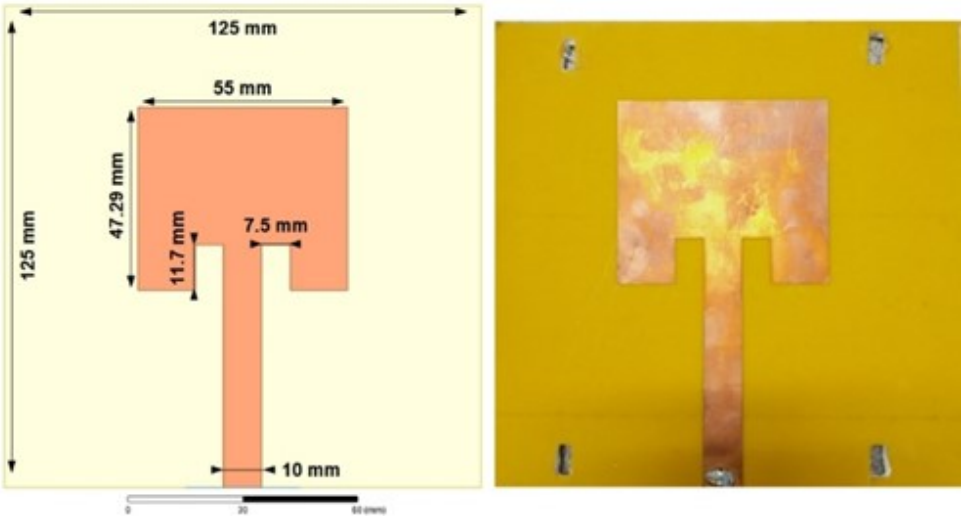

Fig. 3.2. Geometry and dimensions of the simulated antenna (left), and the fabricated antenna on a flat surface (right).

Fig. 3.2 shows the geometry and dimensions of the antenna on the left, and the fabricated antenna on a flat surface on the right. The dielectric properties of the polyimide PCB, provided by the manufacturer, are ε_r = 3.5 and tan δ = 0.002. The dielectric properties of the SSR were determined through a series of experiments as ε_r = 1.54 and tan δ = 0.006.

Three options are considered for the ground plane. In the first option, a polyimide film with 35 μm copper cladding is used. The polyimide film is attached to the SSR with PSA. This solution provides a very good RF ground plane. However, the sandwich of top layer, SSR, and ground plane becomes nearly rigid. For the second option, a flexible copper wire mesh

is used, with a wire diameter 50 μm, and copper coverage of 63%. The third option uses DuPont PE873, which is stretchable silver conductor.
For each option for the ground plane, four configurations are fabricated and tested: on a flat surface, and conformed to cylindrical surfaces with radius R = 160 mm, R = 80 mm, and R = 40 mm. A photo of the patch antenna on these surfaces is shown in Fig. 3.1. The antenna with a copper ground plane on a flat surface is simulated in ANSYS HFSS.

3.3. Measurements

A total of 12 antennas is measured: three ground plane options, and four configurations for each ground plane. The $|S_{11}|$ of all antennas is measured with a Rohde and Schwarz ZVL Vector Network Analyzer and the antenna performance is measured in an anechoic chamber. In the legend of the figures that follow, "Copper" refers to the ground plane made with copper-cladded polyimide, "Mesh" to the copper wire mesh, and "PE873" refers to the ground plane with stretchable silver conductor.
Fig. 3.3 shows the measured $|S_{11}|$ from 2.2 to 2.7 GHz of the antenna on a flat surface for the three ground plane options, as well as the simulated $|S_{11}|$. Good agreement with the simulation is observed for the copper ground plane and the mesh ground plane. For the PE873 ground plane, the frequency of minimum reflection is lowered by 12 MHz and the reflection at that frequency increases. The radiation pattern of the antenna on a flat surface is shown in Fig. 3.4 at 2.45 GHz. The results for the copper ground plane and the wire mesh ground plane are nearly identical and are slightly below the simulated performance. A slight deterioration is observed for the case of the PE873 ground plane. In Fig. 3.5, the realized gain versus frequency is shown. Up to 2.4 GHz the realized gain is nearly the same for the three ground plane options. Above 2.4 GHz, the performance of the PE873 ground plane is slightly lower.

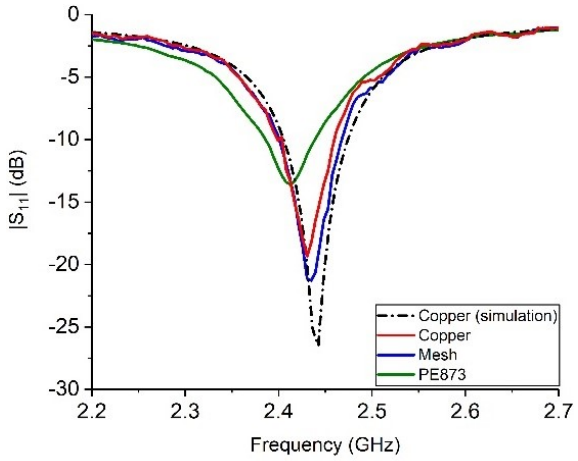

Fig. 3.3. $|S_{11}|$ of the antenna on a flat surface

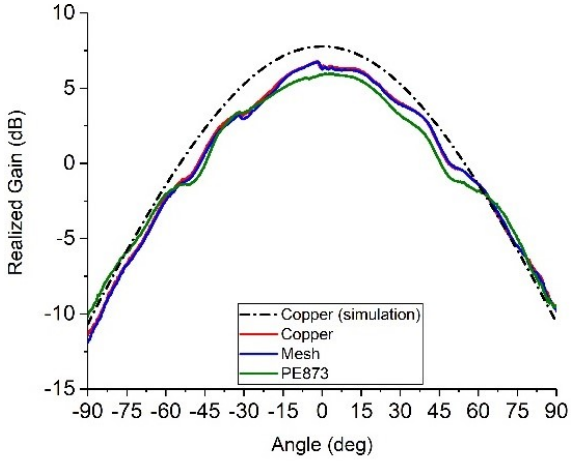

Fig. 3.4. Radiation pattern at 2.45 GHz of the antenna on a flat surface.

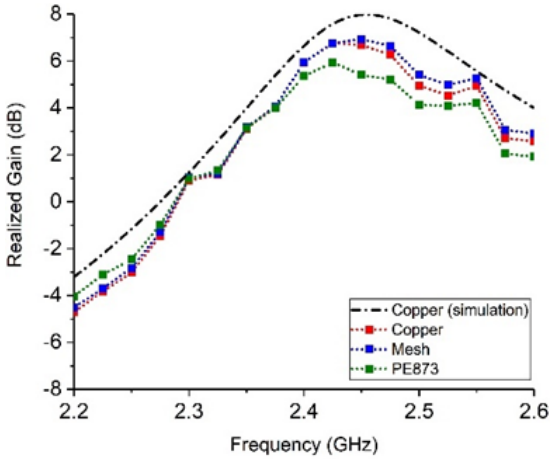

Fig. 3.5. Boresight gain of the antenna on a flat surface.

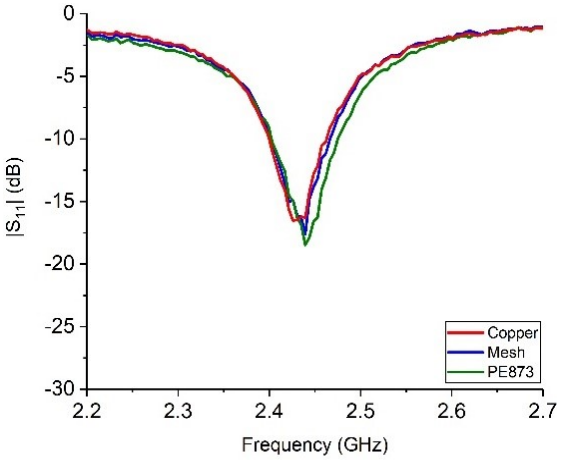

Fig. 3.6. Measured $|S_{11}|$ of the antenna on a cylindrical surface (R = 160 mm).

After measuring the antennas on a flat surface, they are measured when conformed to cylindrical surfaces with radiuses R = 160 mm, R = 80 mm, and R = 40 mm. For the case of R = 160 mm, the measured $|S_{11}|$, radiation pattern, and boresight gain versus frequency are shown in Fig. 3.6, Fig. 3.7. Fig. 3.8, respectively. In this case, the reflection coefficient for the three ground plane options is very similar (Fig. 3.6). The radiation pattern (Fig. 3.7) and the gain (Fig. 3.8) also show very small differences between the three ground plane options.

The measured $|S_{11}|$, radiation pattern, and boresight gain versus frequency for the case of R = 80 mm are shown in Fig. 3.9, Fig. 3.10. Fig. 3.11, respectively. As in the case of R = 160 mm, the differences between the three ground plane options are relatively small. The sidelobes become more pronounced, especially for the wire mesh and the PE873 ground planes.

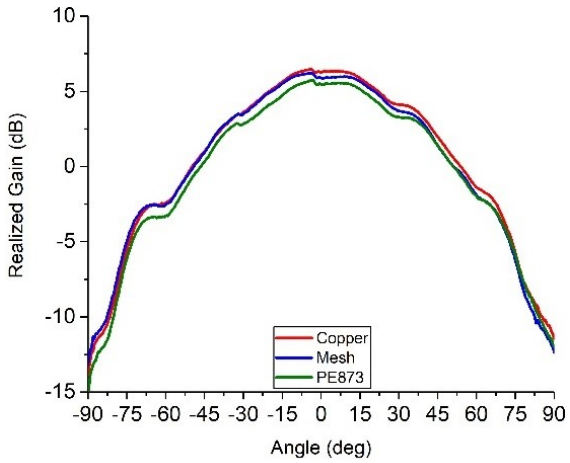

Fig. 3.7. Measured radiation pattern of the antenna at 2.45 GHz on a cylindrical surface (R = 160 mm).

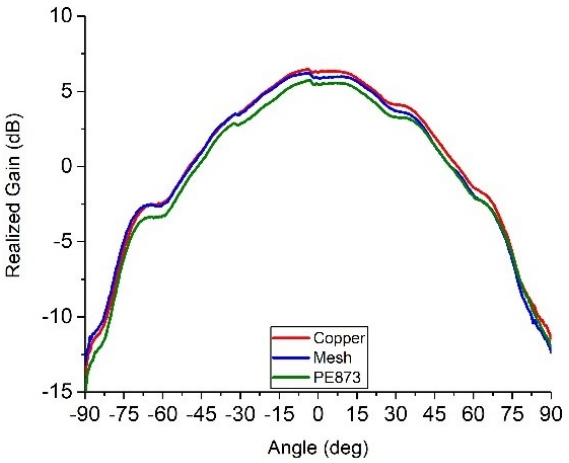

Fig. 3.8. Measured gain of the antenna on a cylindrical surface (R = 160 mm).

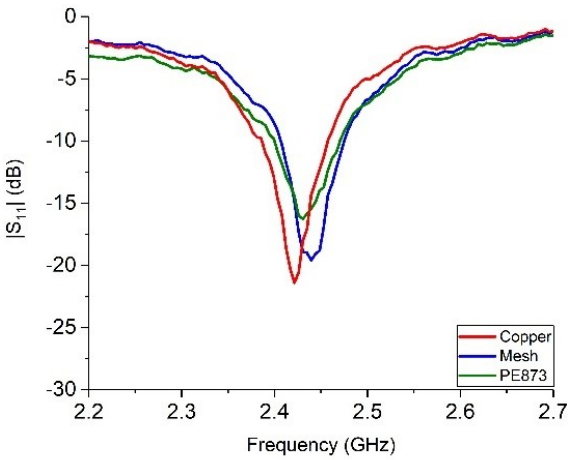

Fig. 3.9. Measured $|S_{11}|$ of the antenna on a cylindrical surface (R = 80 mm).

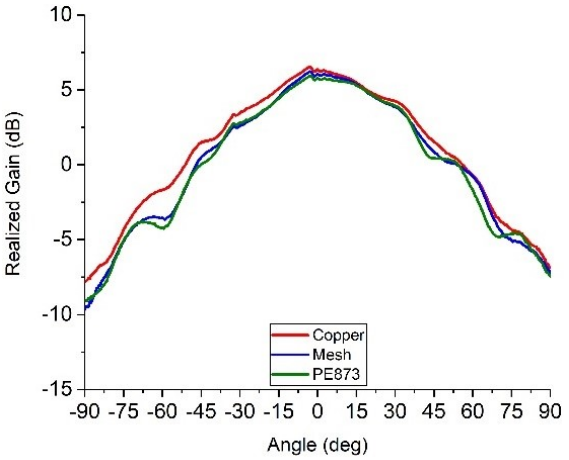

Fig. 3.10. Measured radiation pattern of the antenna at 2.45 GHz on a cylindrical surface (R = 80 mm).

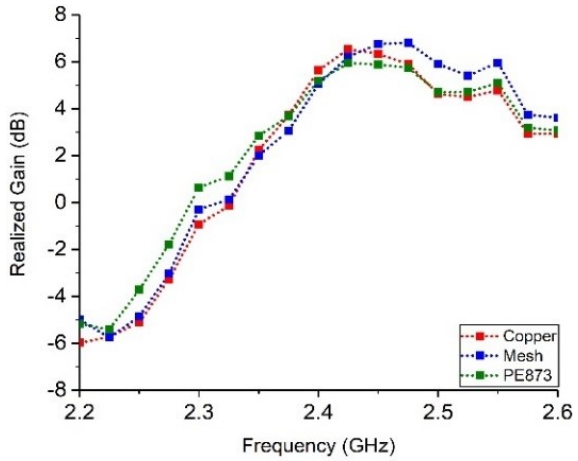

Fig. 3.11. Measured gain of the antenna on a cylindrical surface (R = 80 mm).

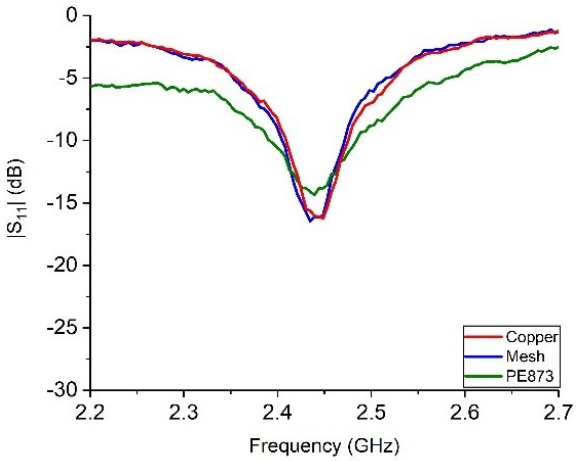

Fig. 3.12. Measured $|S_{11}|$ of the antenna on a cylindrical surface (R = 40 mm).

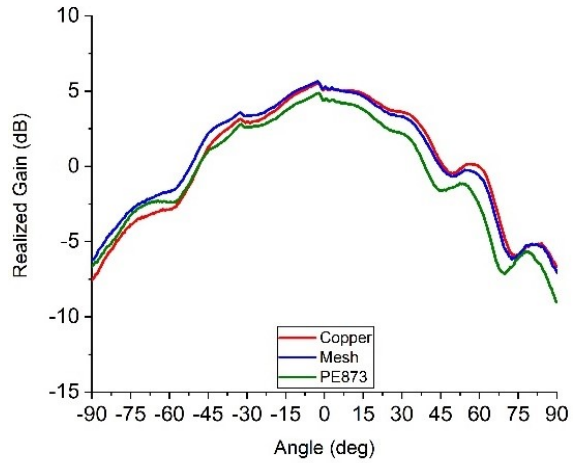

Fig. 3.13. Measured radiation pattern of the antenna at 2.45 GHz on a cylindrical surface (R = 40 mm).

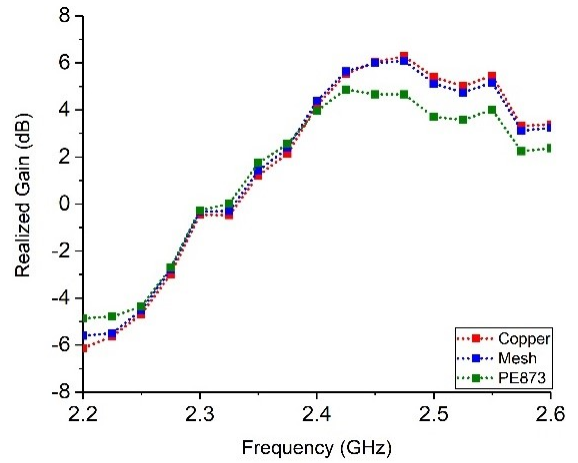

Fig. 3.14. Measured gain of the antenna on a cylindrical surface (R = 40 mm).

Finally, the measured $|S_{11}|$, radiation pattern, and boresight gain versus frequency for the case of R = 40 mm are shown in Fig. 3.12, Fig. 3.13, and Fig. 3.14, respectively. The results for the copper-cladded polyimide ground plane and the copper wire mesh ground plane are virtually the same.

Interestingly, the PE873 ground plane shows significant differences in the reflection coefficient and the radiation characteristics. For all three ground planes, the sidelobes are more pronounced compared to the previous two cylindrical surfaces.

3.4. Discussion

The development of conformable antennas faces many challenges. One such challenge is to maintain flexibility when stacking the different layers on top of each other. Here, the stacking of a polyimide sheet top layer, a SSR sheet for the substrate, and copper-cladded polyimide for the ground plane, results in a rigid antenna. The reason is that the polyimide is flexible, but not stretchable. This antenna can be conformed to a non-planar surface once, and then will remain in that shape. The solution with a copper wire mesh provides slightly more flexibility, without sacrificing much of the antenna performance. The ground plane solution with the PE873 stretchable silver conductor results in an antenna solution that remains flexible. With this ground plane, the antenna performance deteriorates slightly, but certainly not dramatically.

When conformed to non-planar surfaces, the antenna performance is likely to change. Here, the impact of conforming the antenna to cylindrical surfaces is investigated. Comparing the radiation pattern for a flat surface in Fig. 3.4, and the cylindrical surfaces of Fig. 3.7, Fig. 3.10, and Fig. 3.13, a widening of the beam is observed. Similarly, comparing Fig. 3.5, Fig. 3.8, Fig. 3.11, and Fig. 3.14, an increasing reduction in gain is observed when the surface is more curved.

The combination of SSR as substrate, a thin and flexible polyimide PCB for the top layer, and any of the presented ground plane solutions, allows for the development of lightweight and conformable antennas. As shown, the performance of the patch antenna at 2.45 GHz remains relatively stable when the antenna is curved. Further investigations should consider the

performance of SSR as substrate material at higher frequencies. Additionally, as the thermal conductivity of SSR is relatively low, the impact of dissipation and heating should be investigated as well.

3.5. Conclusion

A conformal and lightweight patch antenna for the 2.4 GHz ISM band on silicone sponge rubber (SSR) is presented. The impact on the performance of three different ground plane solutions is investigated: copper-cladded polyimide, copper wire mesh, and DuPont PE873 stretchable silver conductor. For all three cases a flexible, 60 μm thick, polyimide printed circuit board (PCB) is used for the top layer. When placed on a planar surface, the performance of the antenna is very similar for the three ground planes. Subsequently, the impact is measured when conforming the antenna to cylindrical surfaces of radiuses R = 160 mm, R = 80 mm, and R = 40 mm. As the radius of the cylinder decreases, some widening of the beam and some reduction in gain is observed. However, it is found that the performance is not affected in a major way. This technology can be used to develop lightweight and flexible antennas.

Chapter 4. 2x2 Patch array with integrated low noise amplifier

4.1. Introduction

In the previous chapter, a patch antenna was designed and fabricated using silicone sponge rubber as the microwave substrate. The patch antennas itself were fabricated on a commercially available polyimide film, which was attached to the sponge rubber.

Based on this polymer substrate, a low profile microstrip 2x2 patch antenna array with integrated low noise amplifier (LNA) is presented. First, a passive 2x2 patch array is designed and experimentally characterized. Then, the LNA is designed and tested. Finally, the passive array is integrated with the LNA to realize the active array, as shown in Fig. 4.1.

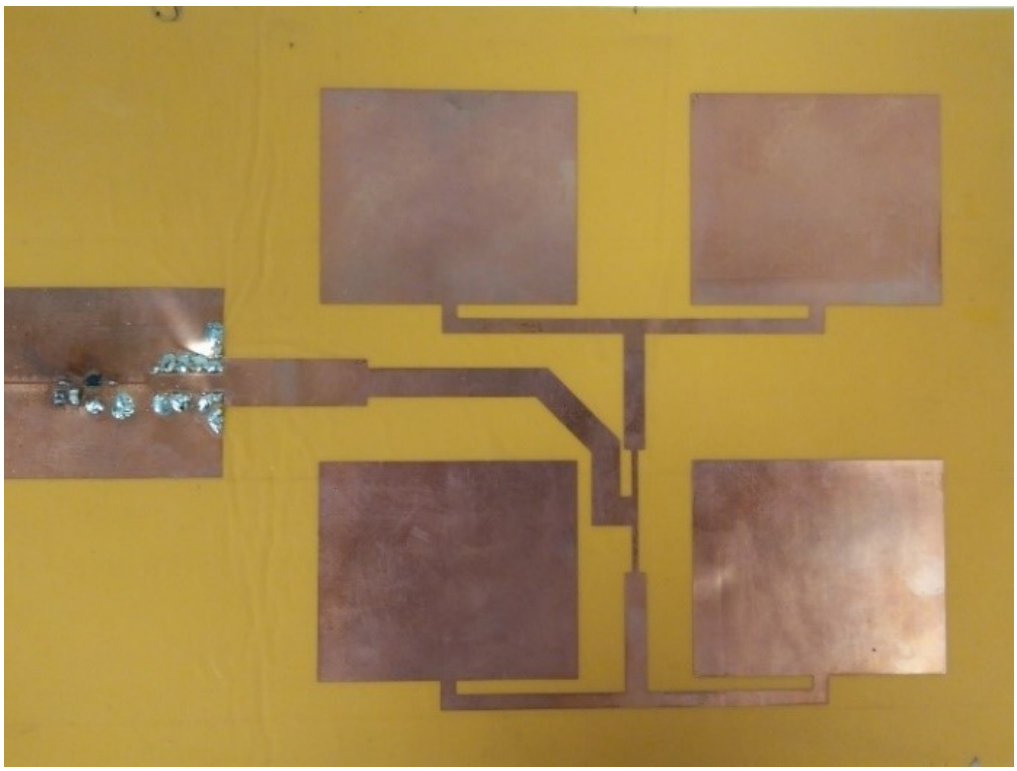

Fig. 4.1. Conformal 2x2 patch array with integrated LNA on silicone sponge rubber.

The performance of the active array is measured on a flat surface, as well as on two cylindrical surfaces. Section 3.2 presents the design, simulated and measured performance of the passive array. Section 3.3 details the design and performance of the LNA circuit on the flexible substrate. Section 3.4 presents the performance of the active array, both in flat and conformed cases. Conclusions are provided in Section 3.5.

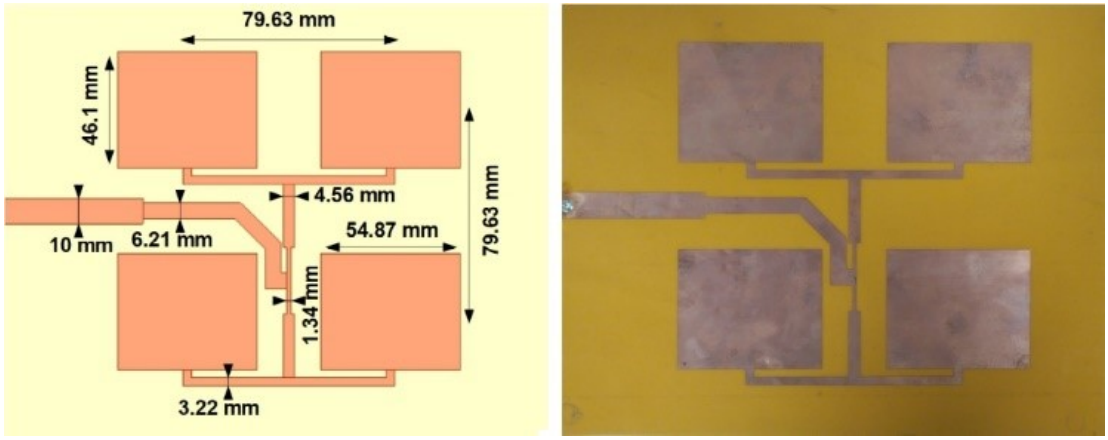

Fig. 4.2. Geometry and dimensions of the passive 2x2 antenna array (left) and the fabricated antenna (right).

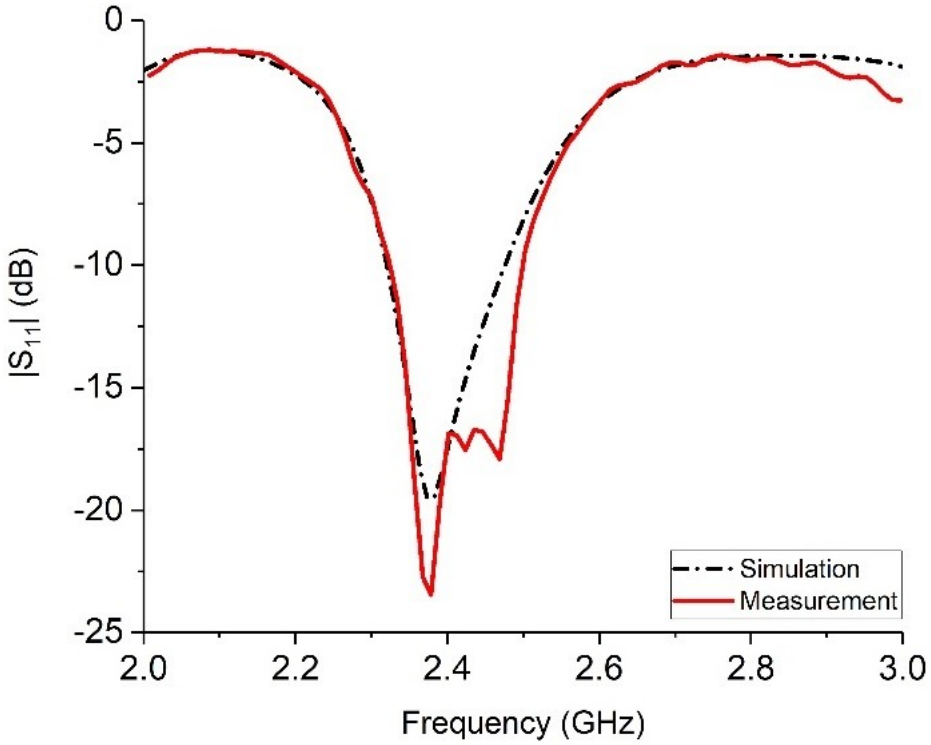

Fig.4.3. $|S_{11}|$ of the passive 2x2 array on a flat surface.

4.2. Passive 2x2 patch array

The patch array is designed for the 2.4 GHz ISM band, which is commonly used for license-free communication systems such as WiFi and Bluetooth. The array consists of 2x2 patches, with the geometry and dimensions shown in Fig. 4.2 on the left. The spacing between patches is 0.64 λ0 and they are vertically polarized. The input impedance of the patches is 106 Ω, and impedance matching to 50 Ω is realized using quarter wavelength transmission lines. The patch array consists of three stacked layers as follows. The top layer is a flexible 60 μm polyimide PCB with copper cladding on both sides. The dielectric properties of the polyimide, provided by the manufacturer, are ε_r = 3.5 and tan δ = 0.002. The patches and the feedlines are realized through standard PCB manufacturing techology. For the the substrate, a 3 mm thick, flexible (11 shore A) sheet of porous SSR is used. The dielectric properties of the SSR are ε_r = 1.54 and tan δ = 0.006 at 2.4 GHz. Pressure sensitive adhesive (PSA) is applied on the back side of the SSR sheet. For the ground plane, a flexible copper wire mesh sheet is used. The wire diameter of the mesh wires is 50 μm, and the percentage of area covered with copper is 63%. The wire mesh is laminated on the back of the SSR sheet, using the PSA. The top PCB is laminated on the SSR sheet using 3M 467MP adhesive.
The patch array on a flat surface is simulated and optimized using ANSYS HFSS. The reflection coefficient $|S_{11}|$ of the patch array on a flat surface is measured with a Rohde and Schwarz ZVL vector network analyzer. The simulated and measured $|S_{11}|$ from 2 GHz to 3 GHz are shown in Fig. 4.3. Good agreement between simulation and measurement is observed.

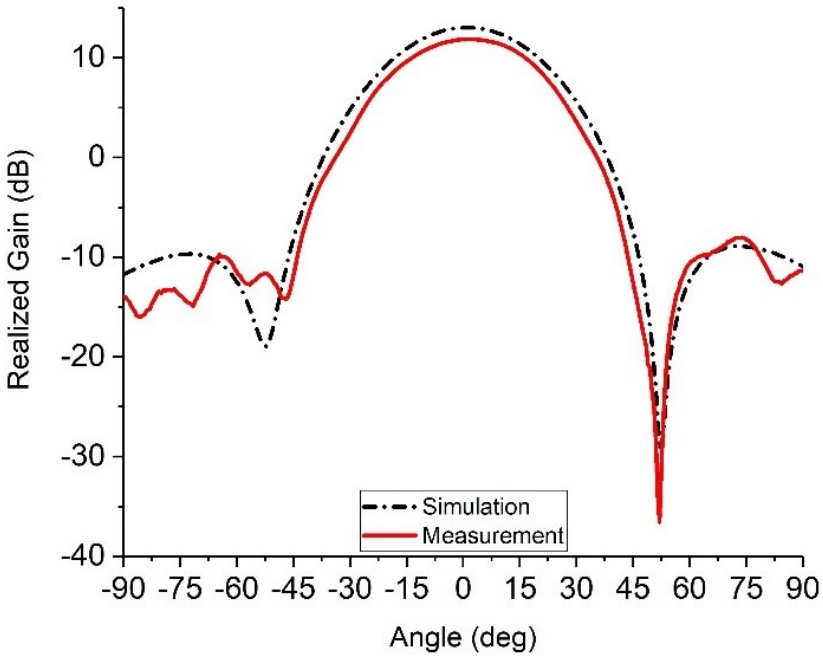

Fig. 4.4. Radiation pattern (H-plane) of the passive 2x2 patch array on a flat surface

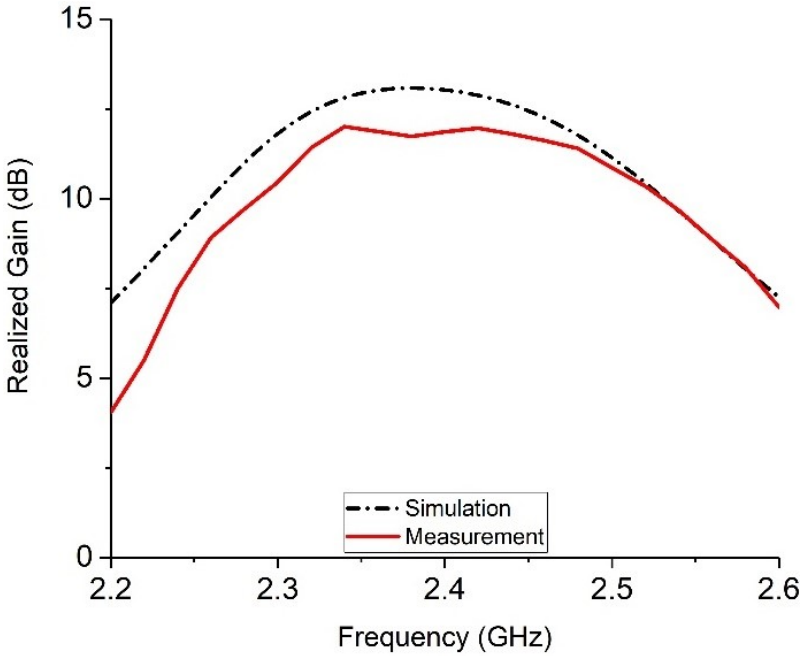

Fig. 4.5. Boresight gain of the passive 2x2 patch array on a flat surface.

The measured bandwidth is 175 MHz (7.3 %), which is slightly larger than the simulated bandwidth of 155 MHz (6.45 %). The antenna performance was measured in an anechoic chamber. Fig. 4.4 shows the simulated and

measured radiation pattern and Fig. 4.5 shows the boresight gain versus frequency. For both measurements, good agreement between simulation and measurement is observed. At boresight, the simulated gain is 13 dB and the measured gain is 11.8 dB.

4.3. LNA on flexible substrate

Next, the LNA is designed on the 60 μm polyimide PCB. The bottom copper cladding of the polyimide PCB serves as ground plane for the grounded coplanar waveguide (GCPW), used in the design of the LNA. The polyimide PCB technology allows for placement of surface-mount devices using conventional surface mount technology. Qorvo's TQP3M9037 was selected for the amplifier [13]. The 50 Ω GCPW output line of the LNA is 115 μm in width. To facilitate the transition from this CPWG line to the width of 10 mm of the microstrip feedline of the passive patch array, a two-stage transition was designed, as shown into Fig. 4.6 (right).

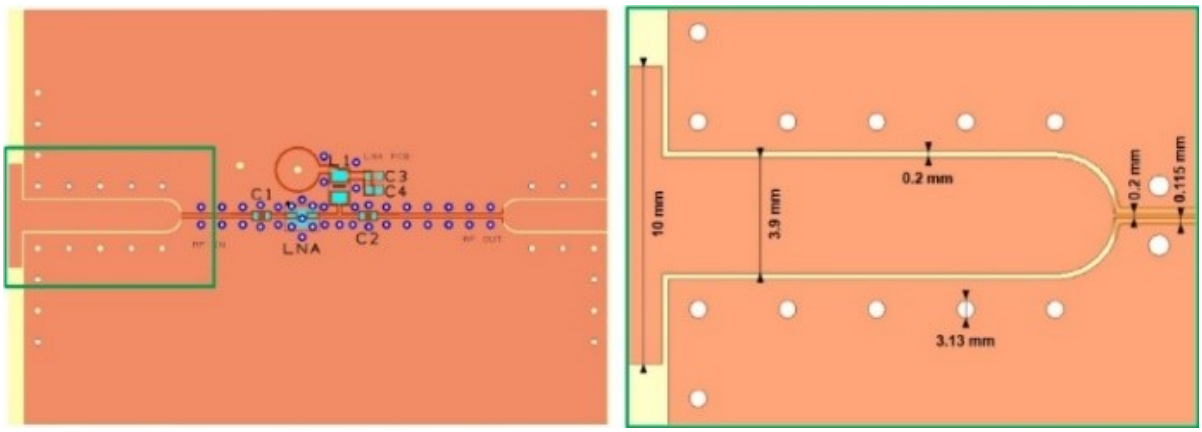

Fig. 4.6. Layout of the LNA (left) and the GCPW to microstrip transition (right).

Fig. 4.7. LNA on flexible substrate (left) and Qorvo evaluation board (right).

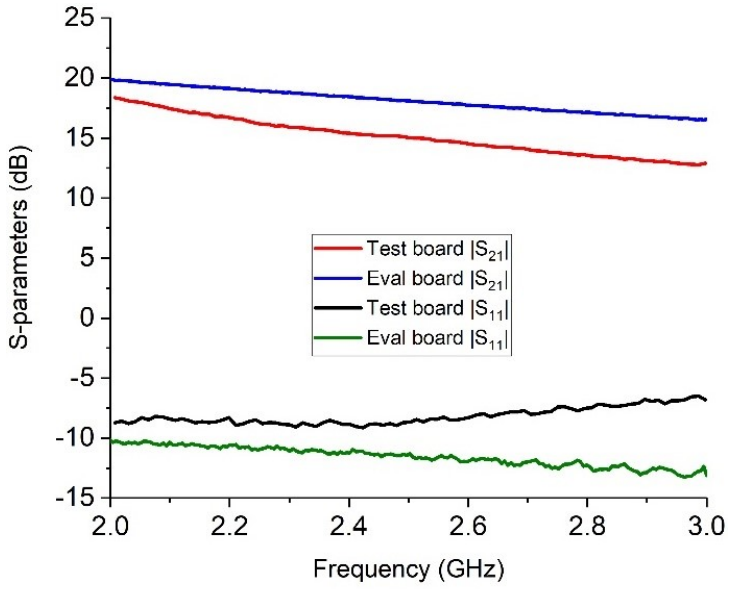

Fig. 4.8. Measured reflection coefficient $|S_{11}|$ and transmission coefficient $|S_{21}|$ for Qorvo's evaluation board and the standalone board on flexible substrate.

First the width of the thin CPWG on the polyimide PCB is increased to a 50 Ω CPW on the 3 mm thick multi-layered substrate, consisting of the polyimide PCB and the SSR substrate. This wider CPW line is then transitioned to the microstrip line. Via holes are added to allow the

ground plane current to flow from the GCPW ground plane to the microstrip ground plane.

Before integrating the LNA with the patch array, a standalone LNA test board was fabricated and measured on the flexible substrate, and its performance compared with Qorvo's evaluation board. The layout of the test board is shown in Fig. 4.6 on the left. Both boards are shown in Fig. 4.7. The measured $|S_{11}|$ and $|S_{21}|$ from 700 MHz to 5 GHz are shown in Fig. 4.8. Decent agreement between simulation and measurement is observed. The measured $|S_{21}|$ of Qorvo's evaluation board at 2.45 GHz is 18.6 dB and the measured $|S_{21}|$ of the standalone board is 15.4 dB. The reduction in gain of 3.2 dB is attributed to the longer length of the transmission lines, the higher losses in the GCPW lines, as well as the imperfect transition from GCPW to microstrip.

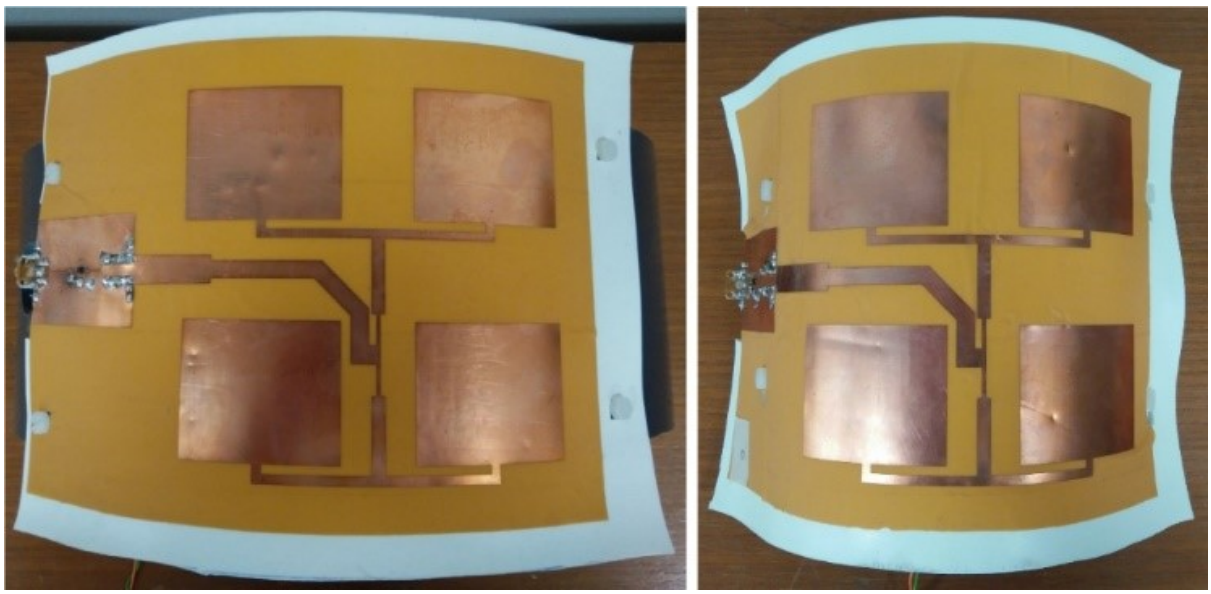

Fig. 4.9. Active 2x2 patch array conformed to a cylinder with radius R = 160 mm (left), and a cylinder with radius R = 80 mm (right).

With these measurement results, an increase in gain of 15.4 dB is expected when the LNA is integrated with the passive 2x2 patch array.

4.4. Active 2x2 conformal patch array on flexible substrate

The last step to develop the active 2x2 patch array is to integrate the LNA with the passive patch array. Additionally, two of the active antennas are conformed to cylindrical surfaces with radiuses of R = 160 mm and R = 80 mm.

The antennas are fabricated using the same methods and technology that were used for the passive array and the LNA, discussed previously. The fabricated active antenna on a flat surface is shown in Fig. 4.1. In Fig. 4.9 the antennas conformed to a cylinder with radius R = 160 mm (left), and a cylinder with radius R = 80 mm (right) are shown.

The performance of the active antennas was measured in an anechoic chamber, with the LNA powered by a 4.8 V battery. Fig. 4.10 shows the measured radiation pattern for the active array, with the results of the passive array included for comparison. And boresight gain versus frequency is shown in Fig. 4.11.

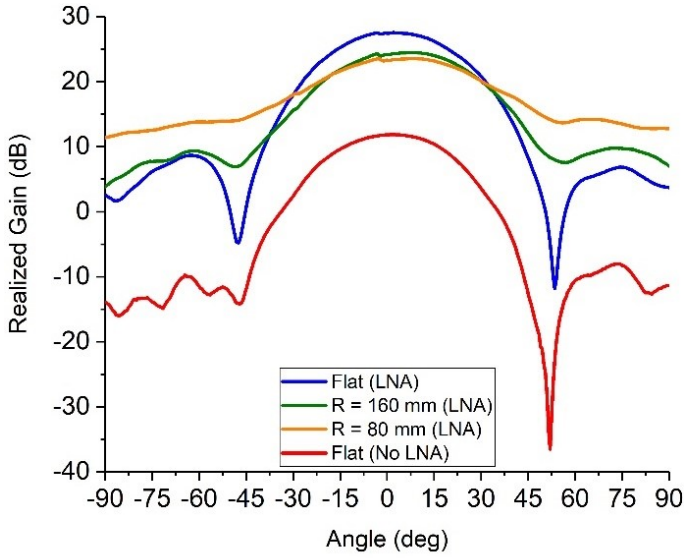

Fig. 4.10. Measured radiation pattern of the active antenna on a flat surface and conformed to cylindrical surfaces with R = 160 mm and R = 80 mm.

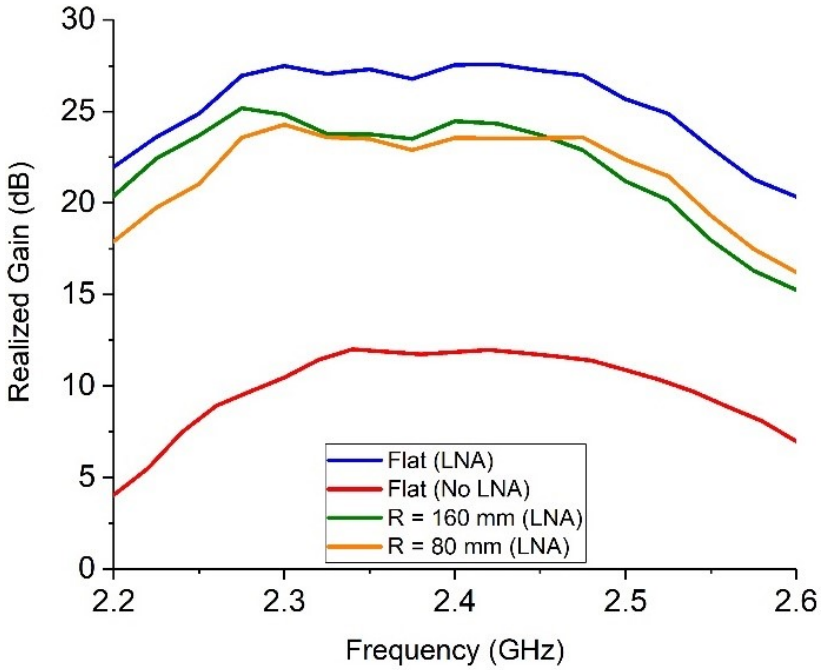

Fig. 4.11. Measured boresight gain of the active antenna on a flat surface and conformed to a cylindrical surface with R = 160 mm, and R = 80 mm.

For the case of the antenna on a flat surface, the measured increase in gain of the active array, compared to the passive array, is 15.6 dB. This increase corresponds well with the anticipated increased in gain of 15.4 dB from the LNA, as discussed in the previous section. Two effects are observed when the active antenna is conformed to the cylindrical surfaces. The first effect is that the boresight gain drops from 27.5 dB for the flat case, to 24.2 dB for the case of R = 160 mm, and to 23.3 dB for the case of R = 80 mm.

4.5. Conclusion

In this chapter, the single patch antenna from the previous chapter was extended to a conformal active 2x2 patch array antenna with an integrated low noise amplifier (LNA). Again a combination of silicone sponge rubber (SSR) for the substrate and flexible polyimide printed circuit board (PCB), with copper cladding on both sides, for the top layer, was used. The ground plane uses a copper wire mesh.

The LNA is realized in the top layer using standard PCB and surface mount technology. The resulting array is very simple to fabricate, easily scalable, lightweight, low profile, and conformable to surfaces.
It was found that the degradation in performance when conforming the antenna to cylindrical surfaces, is limited. The integration of the LNA directly on the flexible PCB demonstrates feasibility of integrating RF functions in a conformal manner directly on the antenna. With these results, it appears feasible to implement more complex functions, such as an entire transmit/receive module.

An important point for further investigations is the thermal management and self-heating of the active circuits, as the silicone substrate has a relatively low thermal conductivity. Consequently, integration of high power components such as a power amplifier, remains a challenge. Specialized flexible polymer substrates loaded with nanoparticles to enhance the thermal conductivity could provide a possible solution.

Chapter 5. Conformal Adaptive Phased Array

5.1. Introduction

Traditionally, phased arrays are realized on planar surfaces. However, there is an increasing need for phased arrays that can be conformed to non-planar surfaces for application in the area of wearables, automotive, and aerospace. These applications often require that such a conformal phased array is lightweight, low-profile, and cost-effective, while maintaining performance similar to a planar phased array. Some applications may even require a phased array which can adapt to changes in the surface it is mounted on. Flexible electronics technology can provide a good solution to most of these design challenges and constraints.

A proof of concept is presented here of a conformal phased array using flexible electronics technology in combination with a low-cost rubber as substrate. The antenna array consists of a linear array of four microstrip patch antennas, selected here for their simplicity of design, fabrication and low profile.

A phased array with a surface faceting approach was demonstrated using thin, semi-flexible Rogers RT/duroid 6002 [1], [2] and Rogers RT/duroid 5880 [14]. A drawback of these substrates is that they must be very thin in order to remain flexible. They also have a relatively high dielectric constant ε_r from 2.3 to 3 and are quite expensive materials, but low loss tangents $\tan \delta < 0.0015$. Polymer as a substrate is a promising candidate for the low microwave region to provide a balance in terms of weight, cost, substrate conformability and flexibility characteristics.

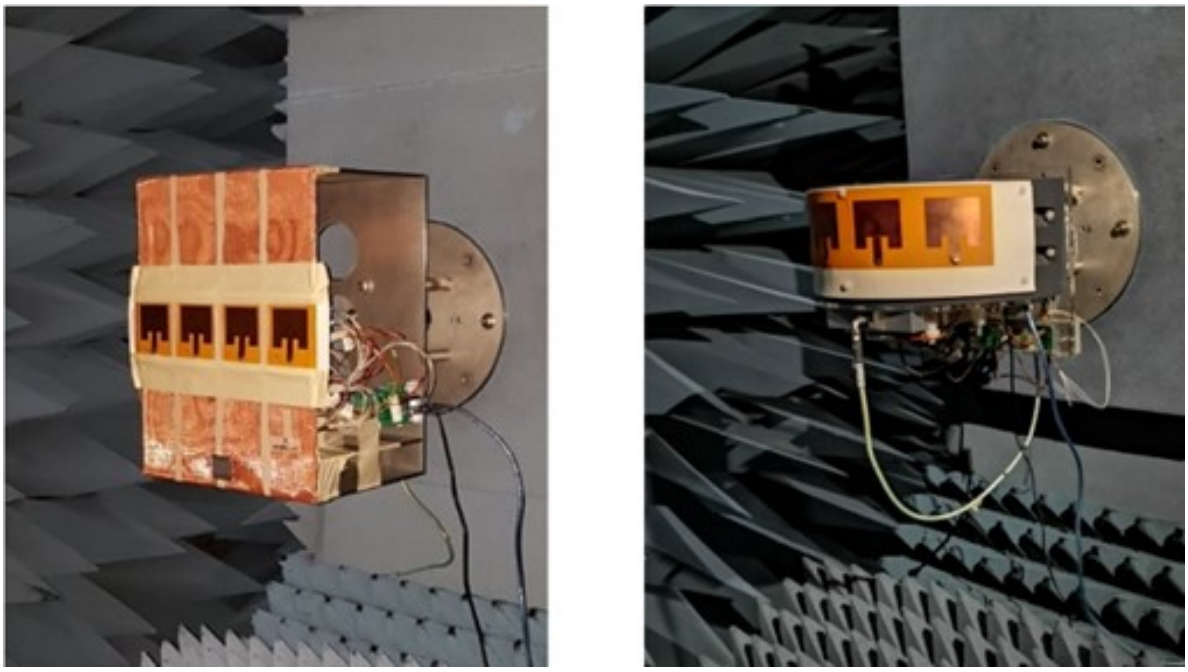

Fig. 5.1. Fabricated phased arrays on a flat surface (left) and conformed to a cylindrical surface with radius R = 160 mm (right).

In Chapter 2, a single patch antenna at 2.4 GHz with silicone sponge rubber was demonstrated. In Chapter 3 a 2x2 patch array with an integrated LNA was presented. In this chapter a conformal array is demonstrated with four patch antennas, realized on a polyimide film using standard PCB techniques, is laminated onto the SSR substrate. Beam steering is realized using vector modulators, which are controlled using an Arduino.

Section 4.2 presents the design and fabrication of the phased array system. In section 4.3 the simulated and measured performance of the phased array on a flat surface is investigated. Section 4.4 presents the performance of the phased array conformed to a cylindrical surface. Finally, conclusions are provided in Section 4.5.

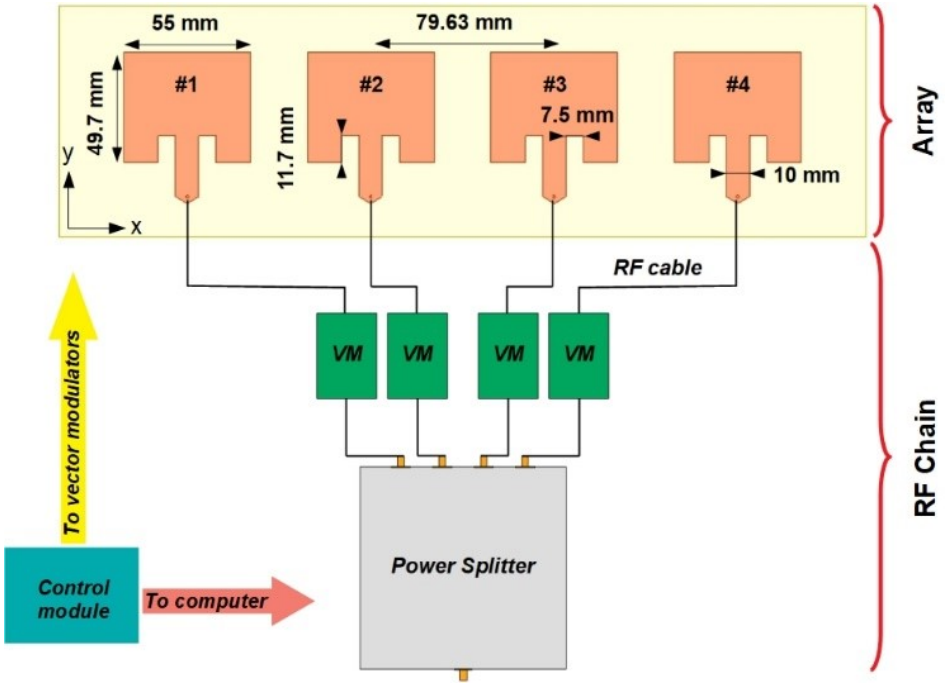

Fig. 5.2. Architecture of the phased array system, including the geometry and the dimensions of the patch array.

5.2. Phased array system

The phased array system is designed for the 2.4 GHz ISM band, which is commonly used for a variety of unlicensed wireless communication applications. The architecture of the phased array system is shown in Fig. 5.2. It comprises a conformal patch array with four patches, vector modulators (VM), a power combiner, and an Arduino controller with a digital to analog converter (DAC) shield and a power distribution shield.
The dimensions of the patch array are also shown Fig. 5.2. The spacing between the elements is 0.64 λ_0 (79.63 mm). On the back side of each patch a 50 Ω SMA connector is placed. The technology of the design uses the same approach as discussed in the previous chapter.

The VM used for phasing each channel is a HMC631LP3 from Analog Devices [15]. The four-way power combiner is a ZB4PD-462W-S+ [16] from Minicircuits. And the system is controlled by an Arduino Uno. Two additional boards are made for power distribution and for digital to analog conversion to directly control the VMs. The phased array system is

controlled through a user interface and control program in MATLAB, running on a laptop communicating with the Arduino controller via USB. Each antenna element of the array is connected to a VM, which, in turn, is connected to the power combiner, all through identical SMA cables. These three stages form the complete RF chain, as shown in Fig. 5.2. The measured insertion loss at 2.4 GHz is 0.97 dB for the power splitting (excluding the 6 dB due to the four-way power splitting), 10.11 dB for the VM, and 2 x 0.36 dB for the two SMA cables. These measured losses are in agreement with the specifications provided by the manufacturers. This makes the total loss of the RF chain 11.8 dB at 2.4 GHz.

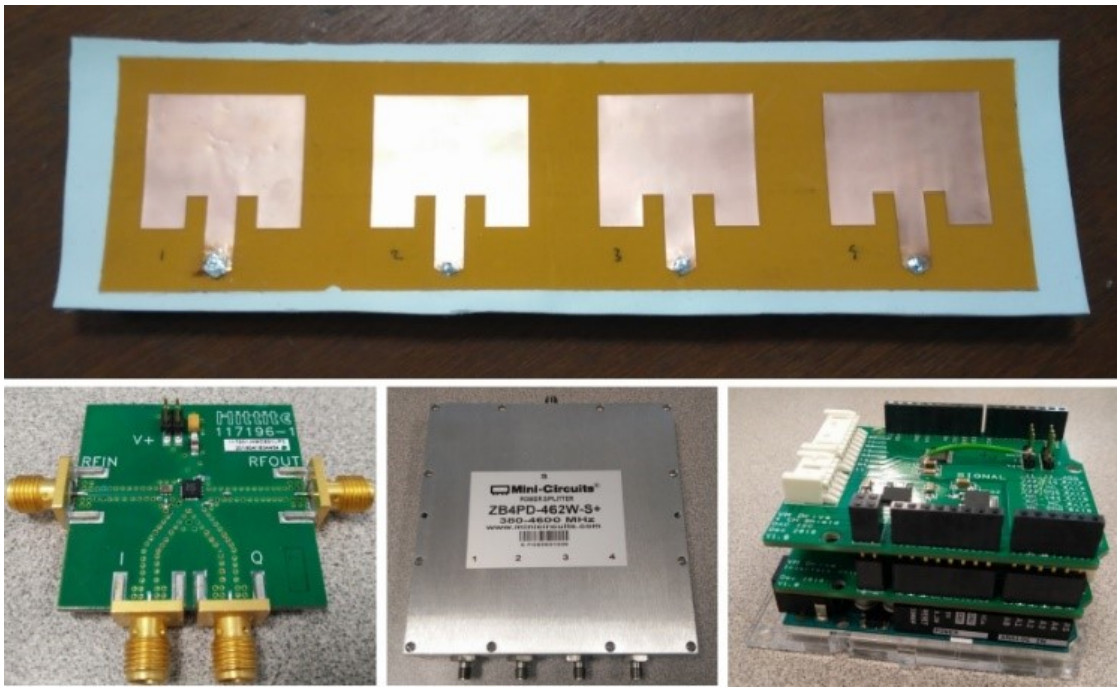

Fig. 5.3. Components of the conformal phased array system: conformal patch array on flexible substrate (top), vector modulator (bottom left), 4-way power splitter (bottom, middle) and Arduino controller stack (bottom, right).

5.3. Phased array on a flat surface

The input reflection coefficient and the radiation pattern of a single element is simulated in HFSS first. This pattern is then used in MATLAB to simulate the whole patch array. The $|S_{11}|$ of each antenna element on a

flat surface was measured with a Rohde and Schwarz ZVL Vector Network Analyzer. The results of the HFSS simulation and the measurement are shown in Fig. 5.4 from 2 GHz to 3 GHz.

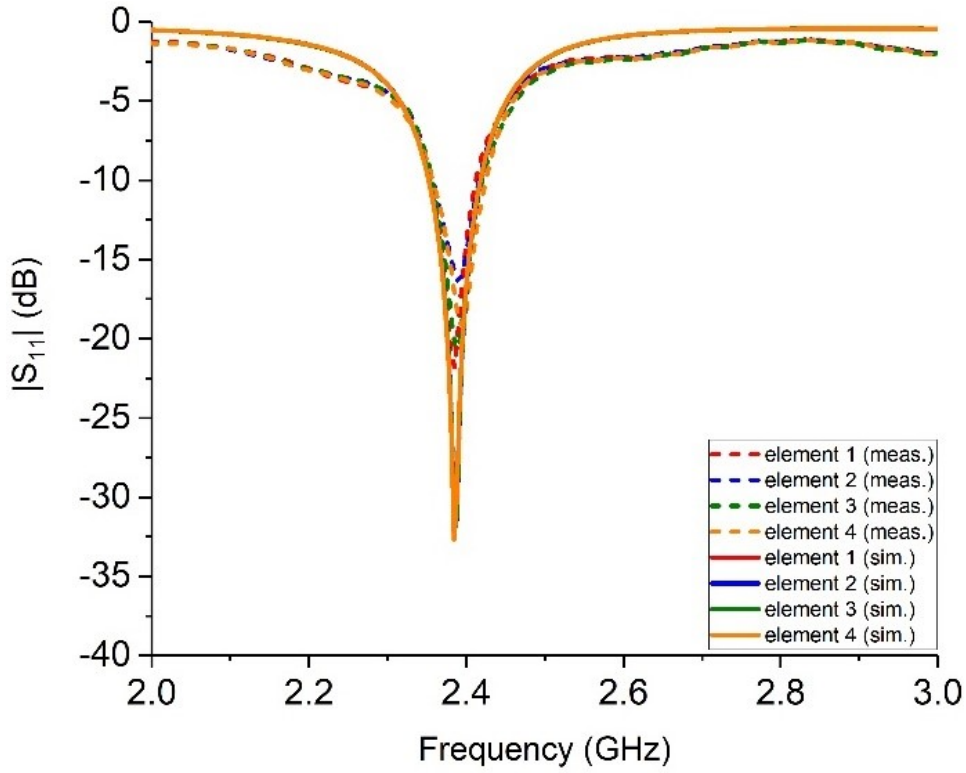

Fig. 5.4. $|S_{11}|$ of the patch array on a flat surface (solid lines: HFSS simulations, dashed lines: measurements).

Good agreement between simulated and measured results is observed. The frequency of minimum reflection of each patch is 2.385 GHz and the measured frequency is 2.392 GHz, i.e., an increase of 7 MHz. The simulated bandwidth is 66 MHz (2.75%), which is close to the measured bandwidth of 67 MHz (2.8 %). Overall, differences between the four elements are small, and differences between simulation and measurement are small as well.

The patch array on a flat surface is simulated with Ansys HFSS and with the phased array toolbox in MATLAB, and its performance was measured in an anechoic chamber.

In Fig. 5.5 the realized gain versus frequency of the patch array on a flat surface is shown. The red trace with the highest gain is the simulated gain of the patch array without the RF chain. The green trace indicates the measured insertion loss of the RF chain, the blue trace represents the simulated gain with the measured RF chain losses subtracted, and the black trace represents the measured boresight gain. At 2.4 GHz the simulated gain is 3.43 dB higher than the measured gain.

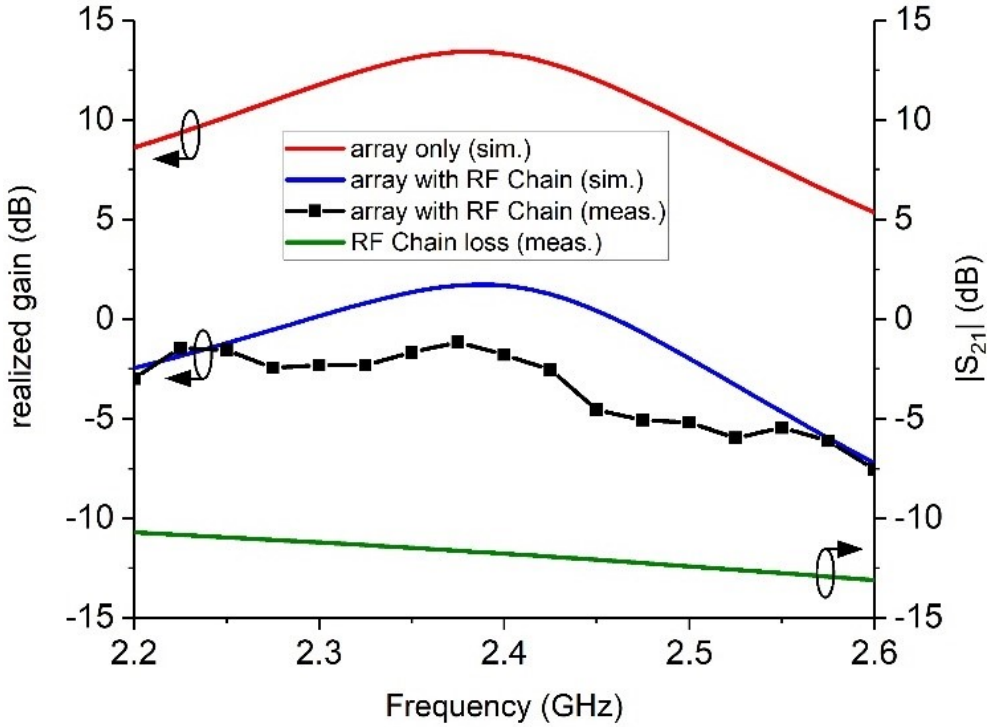

Fig. 5.5. Realized boresight gain of the phased array system (red trace: simulated patch array only, black trace: measured patch array with RF Chain, blue trace: simulated patch array with measured RF Chain, green trace: measured RF Chain loss).

Using the VMs, beam steering of +/- 30° is realized. Limitations in the angular steering span are mostly due to the small number of elements of the array. An angular resolution of 1° is achievable as the VMs are controlled via two voltage levels on the I and Q pins and are not quantified like a typical phase shifter. An advantage of the vector

modulator over phase shifters is their ability to provide amplitude control as well, which provides additional amplitude tapering [17]. The simulated and measured normalized radiation patterns, as function of the azimuth angle θ, are shown in Fig. 5.6 for beam steering at 0 degrees (top), +15 degrees (middle), +30 degrees (bottom). In all cases the gain is normalized to the gain at the steering angle. For all three beam steering cases, good agreement between measurements and HFSS simulations are observed. For angles not too far from boresight, the MATLAB simulations agree with measurements as well. For larger angles, significant differences are observed.

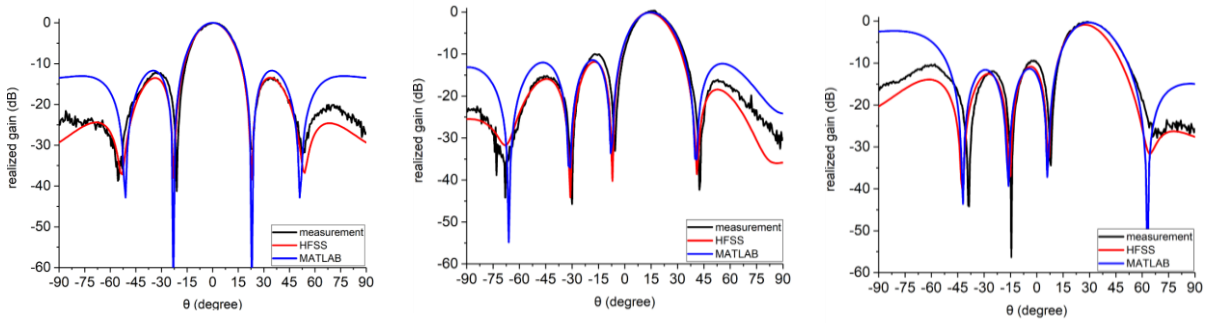

Fig. 5.6. Realized gain (H-plane) of the phased array on a flat surface with beam steering at 0 degrees (left), +15 degrees (middle), and +30 degrees (right) (black trace: measurement, red trace: HFSS simulation, blue trace: Matlab simulation).

5.4. Phased array on a cylindrical surface

In the previous section the antenna elements, the patch array, the RF chain, and the entire phased array were simulated and measured when placed on a flat surface. In this section the performance is investigated with the patch array conformed to a cylinder with radius R = 160 mm, as shown in the photo of Fig. 5.1 on the right. This radius is relatively small, and even leads to "shading", where for large angles from boresight some of the elements are not even visible, as can be seen in Fig. 5.1.

First, the $|S_{11}|$ is measured again with the array conformed to the cylinder. The measured $|S_{11}|$ is shown in Fig. 5.7.

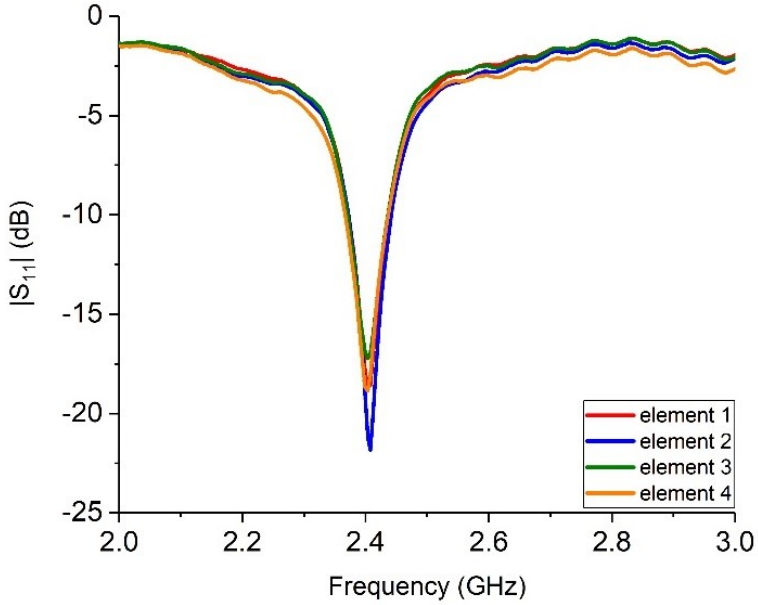

Fig. 5.7. Measured $|S_{11}|$ of each of the four patches with the array conformed to a cylindrical surface with radius R = 160 mm.

The measured frequency of minimum reflection is 2.046 GHz, which is an increase of 14 MHz compared the case of a flat surface. The measured bandwidth is 70 MHz (2.9%), which is close to the case of a flat surface.

Next, the radiation pattern of the phased array is considered. Simulating in HFSS of the patch array conformed to a cylindrical surface proved cumbersome. Instead, the phased array toolbox in MATLAB is used. Modeling of the radiation is relatively easy and for the flat case the toolbox provided good results for angles not too far away from boresight. To illustrate the impact of conforming the antenna to the cylindrical surface, the radiation pattern of the array without phase compensation is shown in Fig. 5.8 (blue trace).

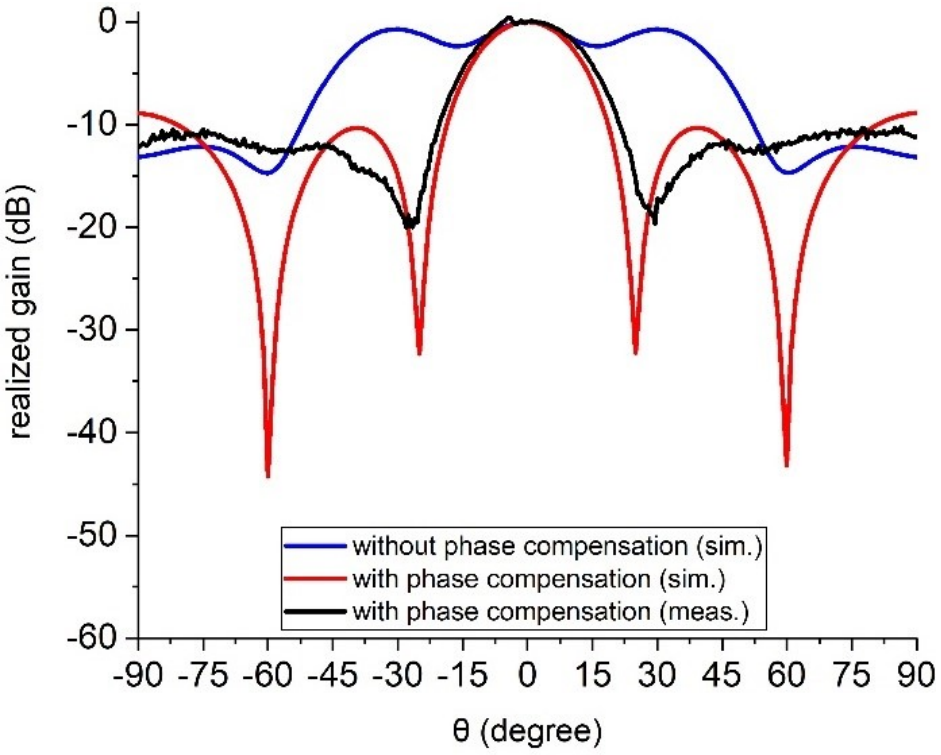

Fig. 5.8. Radiation pattern of the phased array conformed to a cylinder with radius R = 160 mm (blue trace: simulated gain without phase compensation, red trace: simulated gain with phase compensation, black trace: measured gain for system with phase compensation).

Compared to the flat case, the radiation pattern is severely affected. The radiation pattern with phase compensation, compensating for the path length difference between the elements, is shown in the same figure (red trace). The required phasing was also applied to the realized system, and the measured radiation pattern is shown in Fig. 5.8 as well (black trace). The simulated and measured results for the array with phase compensation agree well for angles up to around 30 degrees from boresight. For larger angles significant differences are observed, most notable is the disappearance of the nulls at 60 degrees from boresight.
Using the VMs, beam steering was also investigated. In Fig. 5.9 the measured radiation patterns at 2.4 GHz are shown for beam steering at 0 degrees (top), +15 degrees (middle), and +30 degrees (bottom).

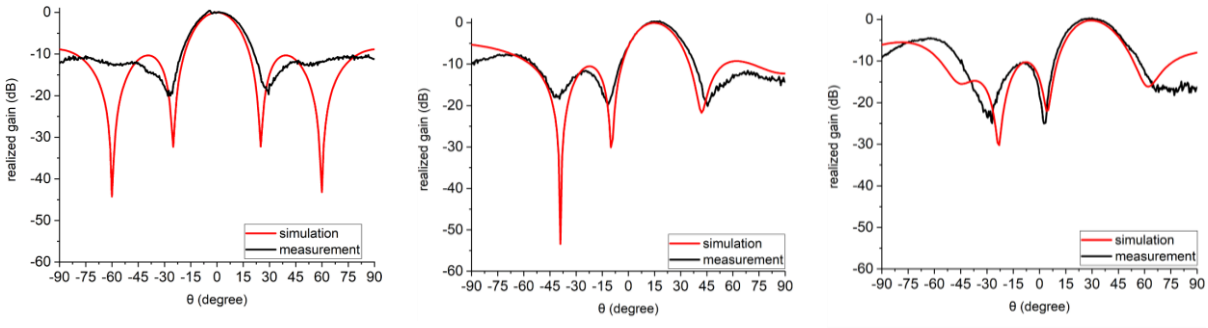

Fig. 5.9. Realized gain of the antenna conformed to a cylindrical surface with radius R = 160 mm (solid line: simulation, dashed line: measurement). Beam steering at 0 degrees (left), 15 degrees (middle), and 30 degrees (right) (red trace: simulation, black trace: measurements).

Very reasonable agreement between measurement and simulation is observed.

An interesting point to note is that the beam width of the main beam increases when the array is conformed to the cylinder, compared to the flat case. This is also predicted by the phased array toolbox in MATLAB. Also, an increase of the side lobe levels is observed compared to the flat case. Both phenomena are illustrated in Fig. 5.10 (left) for beam steering at 0 degrees, and in Fig. 5.10 (right) for beam steering at +30 degrees.

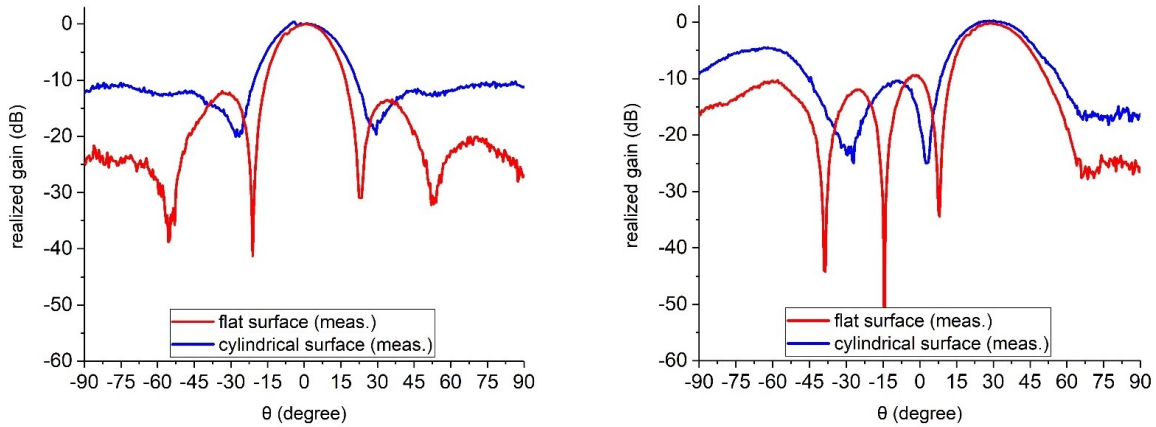

Fig. 5.10: Measured radiation pattern with beam steering at 0 degrees (left) and + 30 degrees (right) (red trace: array on flat surface, blue trace: array on cylindrical surface with radius R = 160 mm).

By looking at the beam width at the -3 dB level and the -10 dB level, a beam widening is observed between +4.75° to +5.25° and +8.5° to +9°, respectively. The measured realized gain versus frequency is shown in Fig. 5.11 for beam steering at 0 degrees for the array on a flat surface (red trace) and for the array conformed to the cylinder. Both curves are very similar in shape, with a drop in gain of 1-2 dB when the antenna is conformed to the cylinder.

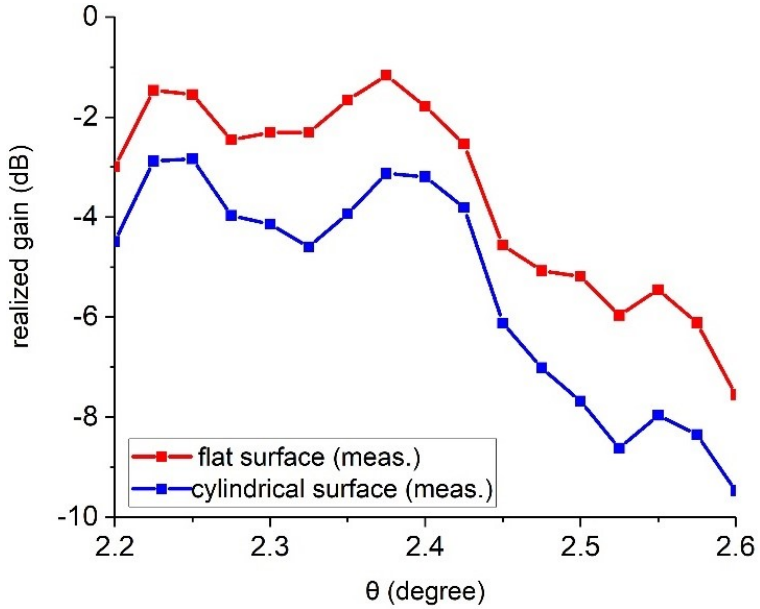

Fig. 5.11. Measured realized gain versus frequency with beam steering at 0 degrees (red trace: array on flat surface, blue trace: array conformed on cylindrical surface with radius R = 160 mm).

5.5. Conclusion

A proof of concept for an adaptive, lightweight, low profile, conformal phased array system for the 2.4 GHz ISM band is presented. The system comprises an array with four patches, vector modulators, a power combiner, and an Arduino controller. The system can easily be scaled to include more elements. The patch array is realized using a polyimide film, with the patches fabricated using standard PCB techniques, a silicone sponge rubber as substrate, and a wire mesh for the ground plane.

The individual patches are first simulated and measured for their input reflection coefficient and radiation pattern. Good agreement is found between simulation and measurement. Subsequently, the phased array is characterized on a flat surface with beam steering. Simulations are performed using ANSYS HFSS and the phased array toolbox in MATLAB. Good agreement is found between HFSS simulations and measurements, and good agreement is observed also with the MATLAB simulations for angles not too far away from boresight. Lastly, the array is conformed to a cylindrical surface with radius R = 160 mm and characterized through MATLAB simulations and measurements.

Very reasonable agreement between simulation and measurement is observed. For larger angles θ from boresight the differences between MATLAB simulations and measurements remain. This is attributed to the fact that the MATLAB simulations do not take into account the "shading" effect, discussed earlier.

The key purpose here is to demonstrate feasibility of the conformal phased array, with phase compensation for the path length differences due to the curving of the surface. It was found that the curved phased array behaves very similar to the flat surface phased array, although boresight gain at 2.4 GHz is reduced by 1.4 dB and the 3-dB beam width increased by 5.25°.

The presented technology can be further expanded to include more antenna elements, with real-time compensation when changes in the shape of the surface occur, which can be measured with appropriate sensors.

Further research is required to assess the impact when all components are integrated on the polyimide film, which is on-going work, and to assess the impact of self-heating, as rubbers have a relatively low thermal conductivity.

Chapter 6. Conclusions and recommendations

6.1. Conclusions

The objective the project is the investigation of feasibility of active phased arrays on flexible substrates.

Various candidates for the microwave substrate were investigated. The substrate discussed in this report is silicone sponge rubber. This material is a rubber with tiny air bubbles. As a result, the material is soft, has a relatively low relative dielectric constant, and a relatively low loss tangent. For the design frequency, the ISM band at 2.4 GHz was used, because of the availability of components and the relatively poor performance of the rubber as microwave substrate at higher microwave frequencies.

In the second chapter, a patch antenna was developed using a polyimide film attached to the sponge rubber. It was found that the performance of the antenna is affected when the antenna is flexed, but that the impact is not large. Also, various ground plane options were investigated: copper on polyimide, copper wire mesh, and DuPont PE873.

In the third chapter, a 2x2 patch array was designed and integrated with a commercially low noise amplifier. It was found that the antenna could be conformed to cylindrical surfaces, with the radiation performance affected due to the bending of the antenna. No impact of the bending on the LNA was observed.

In the fourth chapter, a linear array of four patches was designed using the silicone sponge rubber. Each element of the array was connected to a vector modulator. Measurements demonstrate the feasibility of a flexible array. In this case, the vector modulators were not yet integrated on the flexible substrate. This is left for future work.

6.2. Recommendations

Several flexible materials were investigated in this project for their suitability as microwave substrate. In this report, designs on silicone sponge rubber are presented. This material has a relatively low dielectric constant and low loss tangent at microwave frequencies of a few GHz, while having good strength and flexibility. Given the scope of the project, investigation into suitable materials was limited, and it is recommended that more flexible materials are investigated for their suitability, especially for higher microwave frequencies.

Although not explicitly discussed in detail in this report, it was found the poor thermal conductivity of the flexible substrates poses major challenges when integrating active components on them. For example, attempts were made to integrate a power amplifier on a flexible substrate. However, these investigations were ended due to the relatively high heat generation of the amplifier combined with the poor thermal conductivity. It is recommended that options for flexible materials with a relatively high thermal conductivity are investigated. Materials research could bring benefits in this area. Also, smart designs may help to create thermally conducting channels in the designs, which may help alleviate the thermal problems.

The frequency of operation for the designs in this report is at 2.4 GHz. This choice was motivated by the availability of the necessary components and the relatively good performance of the rubber substrate at that frequency. It is recommended that materials and designs at higher frequencies are further investigated.

Commercially available components are used in the designs in this project. These components are attached to the polyimide films using commercially available PCB techniques. Bending the substrate may result

in mechanical stresses, which may cause breaks in the soldering joints or even the components itself. It is recommended that new technologies are explore in which the integrated circuits are developed directly on a flexible substrate.

In this report the antennas are conformed to cylinders, which is relatively straightforward case requiring only bending of the substrates. It is recommended that materials and designs are investigated that will be conformed to more complicated surfaces, such as spheres.

References

[1] B. D. Braaten et al., "Phase-Compensated Conformal Antennas for Changing Spherical Surfaces," IEEE Trans. Antennas Propag., vol. 62, no. 4, pp. 1880–1887, 2014.

[2] B. D. Braaten et al., "A self-adapting flexible (SELFLEX) antenna array for changing conformal surface applications," IEEE Trans. Antennas Propag., vol. 61, no. 2, pp. 655–665, 2013.

[3] M. A. Aziz, S. Roy, L. A. Berge, Irfanullah, S. Nariyal, and B. D. Braaten, "A conformal CPW folded slot antenna array printed on a Kapton substrate," in Proceedings of 6th European Conference on Antennas and Propagation, EuCAP 2012, 2012, pp. 159–162.

[4] A. S. M. Alqadami, M.F. Jamlos, P. J. Soh, G. A. E. Vandenbosch, "Assessment of PDMS Technology in a MIMO Antenna Array," IEEE Antennas Wirel. Propag. Lett., vol. 15, pp. 1939–1942, 2016.

[5] T. Jang, C. Zhang, H. Youn, J. Zhou, and L. J. Guo, "Semitransparent and flexible mechanically reconfigurable electrically small antennas based on tortuous metallic micromesh," IEEE Trans. Antennas Propag., vol. 65, no. 1, pp. 150–158, 2017.

[6] B. S. Cook, B. K. Tehrani, J. R. Cooper, and M. M. Tentzeris, "Multilayer Inkjet Printing of Millimeter-Wave Proximity-Fed Patch Arrays on Flexible Substrates," IEEE Antennas Wirel. Propag. Lett., vol. 12, no. X, pp. 1351–1354, 2013.

[7] W. T. Li, Y. Q. Hei, P. M. Grubb, X. W. Shi, and R. T. Chen, "Inkjet Printing of Wideband Stacked Microstrip Patch Array Antenna on Ultrathin Flexible Substrates," IEEE Trans. Components, Packag. Manuf. Technol., vol. 8, no. 9, pp. 1695–1701, 2018.

[8] B. Sanz-Izquierdo, S. Jun, J. Heirons, and N. Acharya, "Inkjet printed and folded LTE antenna for vehicular application," Eur. Microw. Week 2016 "Microwaves Everywhere", EuMW 2016 - Conf. Proceedings; 46th Eur. Microw. Conf. EuMC 2016, pp. 88–91, 2016.

[9] M. Rizwan, M. W. A. Khan, L. Sydanheimo, J. Virkki, and L. Ukkonen, "Flexible and Stretchable Brush-Painted Wearable Antenna on a Three-Dimensional (3-D) Printed Substrate," IEEE Antennas Wirel. Propag. Lett., vol. 16, pp. 3108–3112, 2017.

[10] R. Quarfoth, Y. Zhou, and D. Sievenpiper, "Flexible Patch Antennas Using Patterned Metal Sheets on Silicone," IEEE Antennas Wirel. Propag. Lett., vol. 14, pp. 1354–1357, 2015.

[11] Z. Li et al., "Rational design of a printable, highly conductive silicone-based electrically conductive adhesive for stretchable radio-frequency antennas," Adv. Funct. Mater., vol. 25, no. 3, pp. 464–470, 2015

[12] DuPont, "DuPont PE873 – Stretchable silver conductor". https://www.dupont.com/content/dam/Dupont2.0/Products/Electronics-and-imaging/Literature/PE873.pdf, 2014.

[13] QORVO, "TQP3M9037 - Ultra Low-Noise, High Linearity LNA," pp. 1–16, 2017.

[14] Y. Xia, B. Muneer, and Q. Zhu, "Design of a Full Solid Angle Scanning Cylindrical-and-Conical Phased Array Antennas," IEEE Trans. Antennas Propag., vol. 65, no. 9, pp. 4645–4655, 2017.

[15] ANALOG DEVICES, "HMC631LP3 / 631LP3E GaAs HBT Vector Modulator," pp. 1–8.

[16] Minicircuits, "Power Splitter / Combiner ZB4PD-462W+," pp. 1–2.

[17] Irfanullah, S. Khattak, and B. D. Braaten, "Improvement of the broadside radiation pattern of a conformal antenna array using amplitude tapering," Appl. Comput. Electromagn. Soc. J., vol. 32, no. 6, pp. 511–516, 2017.